

---

# EEG SOURCE LOCALIZATION ANALYSIS IN EPILEPTIC CHILDREN DURING A VISUAL WORKING-MEMORY TASK.

---

A PREPRINT

**Galaris Evangelos**

Dipartimento di Matematica e Applicazioni “Renato Caccioppoli”  
Universita’ di Napoli Federico II  
Naples, Italy

**Gallos Ioannis**

School of Applied Mathematics and Physical Sciences  
National Technical University of Athens  
Athens, Greece

**Myatchin Ivan**

Department of Anesthesiology  
Sint-Trudo Regional Hospital  
Sint-Truiden, Belgium

**Lagae Lieven**

Department of Development and Regeneration  
Section Paediatric Neurology, KULeuven  
Leuven, Belgium

**Siettos Constantinos**

Dipartimento di Matematica e Applicazioni “Renato Caccioppoli”  
Universita’ di Napoli Federico II  
Naples, Italy

(Corresponding author, constantinos.siettos@unina.it)

May 25, 2020

## ABSTRACT

We localize the sources of brain activity of children with epilepsy based on EEG recordings acquired during a visual discrimination working memory task. For the numerical solution of the inverse problem, with the aid of age-specific MRI scans processed from a publicly available database, we use and compare three regularization numerical methods, namely the standardized Low Resolution Electromagnetic Tomography (sLORETA), the weighted Minimum Norm Estimation (wMNE) and the dynamic Statistical Parametric Mapping (dSPM). We show that all three methods provide the same spatio-temporal patterns of differences between epileptic and control children. In particular, our analysis reveals statistically significant differences between the two groups in regions of the Parietal Cortex indicating that these may serve as “biomarkers” for diagnostic purposes and ultimately localized treatment.

**Keywords** Source Localization · Neuroimaging · Epilepsy · Children

## 1 Introduction

Epilepsy affects more than 65 million people worldwide while, approximately 1 out of 150 children is diagnosed with epilepsy during the first 10 years of their life [1]. Although many children self-heal before adulthood, it has been shown that children with epilepsy confront various cognitive and behavioural problems such as problems in learning, attention and memory capacity [2]. Thus, the systematic study of the brain (dys)functionalities of children with epilepsy, and ultimately the development of efficient/targeted treatments is one of the most challenging problems in neuroscience and beyond. Towards this aim, non-invasive neuroimaging techniques and in particular electroencephalograph (EEG) recordings are commonly used for clinical assessment [3–10]. However, an analysis at the scalp level does not give insight to the malfunctioning of the actual brain regions and/or their connectivity. On the other hand, fMRI analysis can provide a better insight but it is limited by its low-time resolution. Thus, source localization, i.e. the identification of brain regions from scalp/non-invasive recordings (usually EEG or MEG) has emerged a promising approach that can facilitate the analysis of brain activity as a clinical diagnostic tool [11, 12]. However, the source localization problem is an ill-defined problem and as such, it poses open questions regarding its robustness and in general the validity of the obtained results [13]. Thus, comparative studies between the various numerical methods that aspire to solve the source localization problem are critical [14, 15]. Toward this aim, Jatoi et al. [16] have compared the standardized low resolution brain electromagnetic tomography (sLORETA) with the exact LORETA (eLORETA) based on EEG recordings of a visual experiment on healthy subjects. Cincotti et al. [17] compared two techniques for source localization, namely the surface Laplacian and LORETA using EEG recordings from a group of Alzheimer disease patients and age-matched controls. Yao and Devald [18] compared the performances of several source localization methods on the basis of both simulated and experimental EEG data of somatosensory evoked potentials. Attal and Schwartz [19] compared the performance of three methods, namely the weighted minimum norm (wMNE), sLORETA and the dynamic statistical parameter mapping (dSPM) for the characterization of distortions in cortical and subcortical regions using a realistic anatomical and electrophysiological model of deep brain activity. Seeland et al. [20] compared wMNE, sLORETA and dSPM using EEG data taken from eight subjects performing voluntary arm movements.

Regarding epilepsy, the majority of the studies have performed source localization with the aid of EEG-fMRI recordings and/or simulated data approximating epileptic spatio-temporal patterns such as spikes and discharges. For example, Ioannides et al. [21] assessed the performance of two source localization methods, wMNE and eLORETA using MEG signals of ictal and interictal epileptiform discharges in epilepsy and K-complexes. Chowdhury et al. [22] compared the performance of the coherent Maximum Entropy on the Mean (cMEM) and the 4th order Extended Source Multiple Signal Classification (4-ExSo-MUSIC) using MEG and EEG synthetic signals mimicking normal background and epileptic discharges. Hasan et al. [23] evaluated four algorithms (dSPM, wMNE, sLORETA and cMEM) using simulated data from a combined biophysical/physiological model used to generate interictal epileptic spikes as well as real EEG data recorded from one epileptic patient who underwent a full presurgical evaluation for drug-resistant focal epilepsy. Moeller et al. [15] provides a review of the studies that used EEG-fMRI recordings to assess different types of epileptic form activity, underpinning the necessity for comparing with other methods including EEG source analysis.

Fewer studies have dealt with source-level analysis and compared different source localization methods using EEG clinical data taken by children with epilepsy. Among these studies, Adebimpe et al. [24] performed source localization using eLORETA to investigate changes in functional connectivity in children with Benign rolandic epilepsy with centrotemporal spikes using resting-state EEG recordings. Groening et al. [25] combined EEG-fMRI and EEG source analysis to identify epileptogenic foci in children. Elshoff et al. [26] examined the efficiency of EEG-fMRI and EEG source analysis to localize the point of seizure onset in children with refractory focal epilepsy.

The above studies have focused mainly on the study of brain regions that are activated during seizure periods or before their onset. Several other studies have also aimed at analyzing the emerged patterns during seizure periods. For example, Fergus et al. [27] used a supervised machine learning approach to classify seizure and non-seizure records using an open dataset of seized EEG signals from both children and adults.

On the other hand, it has been shown, that studying epileptic seizure-free EEG recordings is of great importance as such analysis can facilitate the identification of patients at risk of epilepsy and/or forecast forth-coming seizures (for a discussion and review of ictal and interictal activity and their analysis see for example [10]).

Here, we perform a source-localization analysis of the brain activity of well-controlled epileptic children during a visual Working Memory (WM) task. WM is commonly viewed as a functional integration system with limited capacity that is able to store information within a short-term register and simultaneously manipulate it on-line. Thus, WM is one of the most important components of information processing and its dysfunction leads to various problems in several cognitive functions including mental arithmetic [28], reading [29, 30], decision making [31] and reasoning [32]. Epilepsy affects a lot the WM functioning as it has been shown by many studies [33–37].

Here, for the solution of the inverse problem, we use three methods, namely, sLORETA [38], dSPM [39] and wMNE [40]. A statistical comparative analysis between methods and groups (healthy children vs children with epilepsy) revealed the crucial role of the Superior Parietal Lobule (SPL) and Inferior Parietal Lobule (IPL) at WM. Our findings are in line with fMRI studies [41–44] that have shown that SPL and IPL are being involved in WM processing and thus can serve as a “biomarker” for identifying, monitoring and assessing epilepsy in children.

## 2 Materials and methods

### 2.1 Experimental Procedure

#### 2.1.1 Subjects

In the study group, 21 children with established childhood epilepsy (age 6—16 years old; mean 11.43 years,  $SD \pm 2.3$ , 10 boys) were enrolled. These children were diagnosed with one out of two following epilepsy syndromes: benign rolandic epilepsy (BRE) ( $n = 9$ ) and idiopathic generalized epilepsy (GE) ( $n = 12$ , including childhood absence epilepsy ( $n = 5$ ) and generalized epilepsy with tonic-clonic seizures ( $n = 7$ )). All children were admitted to the neurophysiology laboratory of the University Hospital of Leuven for a 24-h video-EEG monitoring during which the ERP study was done. They had no anti-epileptic treatment ( $n = 3$ ) or were on standard anti-epileptic medication (monotherapy,  $n = 15$ , duotherapy,  $n = 3$ ), with drug dosages always being within normal ranges. Patients on monotherapy received valproic acid ( $n = 7$ ), carbamazepine ( $n = 4$ ), lamotrigine ( $n = 3$ ) or sulthiame ( $n = 1$ ). Patients on duotherapy received different drug combinations [7]. None of the patients had structural brain abnormalities; in 18 patients, brain MRI was performed showing normal findings in all cases. Only patients with at least an eight days seizure-free period preceding the test were included [7]. Thereby we could avoid an acute effect of epileptic seizures on the child’s performance. All children followed mainstream school and none had a history of learning problems. As a control group, 25 age-matched non-epileptic children (mean age 10.76 years,  $SD \pm 3.4$ , 17 boys) were selected, who did not have any school problem either. The study protocol was approved by the Ethical Committee of University Hospital of Leuven. For more details about the experimental procedure please see Myatchin et al. [7].

#### 2.1.2 Design and Stimuli

The event-related potentials study was done as part of video-EEG monitoring. A visual one-backmatching working memory task was performed: children observed a continuous stream of seven different figures presented one after the other in pseudorandom order at the middle of a computer monitor, which was located at a distance of 1.0m from the subject’s eyes. Everyday figures were used (horse, wardrobe, jacket, cake, comb, bunch of grapes, hammer), white with a black contour on grey background, size 7.5 cm  $\times$  6.5 cm, visual angle  $4^\circ 18' \times 3^\circ 02'$ . Each stimulus was presented for 1.5 s, followed by a delay of 1.0 s, after which the next stimulus was presented. During the delay period a fixation point (dark-grey cross) was shown at the middle of the screen to facilitate eyes fixation. Any figure identical to the one immediately preceding it was defined as a target stimulus (probability 0.30). Children were asked to respond to all targets by pressing a button with their dominant hand. Both accuracy and speed were stressed. The single experimental block contained 120 trials, 36 of which were targets. The duration of the block was 5 min. This is an easy working memory task, which was chosen to ensure a good level of participant’s performance.

First, the electrode placement and impedance calibration was performed. After that, the experimental procedure was described to the child. The child was seated comfortably in a dimly lit registration room and was instructed to look at the middle of the computer screen placed in front of him to avoid unnecessary eye movements; a fixation point (dark-grey cross) was shown between figures to facilitate eye fixation. The child was also instructed to avoid movements to reduce muscle artifacts in the EEG signal. The instruction for the task was given directly before the task. During the experiment, no interaction with the experimenter was allowed during the task and the experimenter sat out of sight of the child.

#### 2.1.3 EEG recordings

Nineteen Ag/AgCl electrodes (Technomed Europe) were placed according to the international 10-20 system at Fp1, Fp2, F3, F4, F7, F8, Fz, C3, C4, Cz, T3, T4, T5, T6, P3, P4, Pz, O1 and O2. Placement of additional four EOG electrodes resulted in two EOG channels: horizontal EOG – two electrodes on the outer canthi of eyes, and vertical EOG – two electrodes above and below one eye. EOG channels allowed us to detect both vertical and horizontal eye movements in order to effectively remove them from EEG recording during subsequent preprocessing of the signal (see below). Two linked mastoid electrodes were used as a reference. EEG was sampled at a frequency of 1000 Hz with 12 bits A/D converter and amplified using a band-pass filter of 0.095 – 70 Hz. Notch filter was off. Registration of the digital EEG was made using the software program Brainlab 4.0 (OSG, Belgium). The impedance of all electrodes was

monitored for each subject prior to recording and was always kept below 5 k $\Omega$ .

### 2.1.4 Data pre-processing

Data pre-processing was performed offline using the EEGLAB v.5.02 toolbox (Matlab 7.0.4 platform) [45]. The ECG channel was factored out. Data were filtered with a 50 Hz digital low pass filter. Eye movement artifacts were marked and removed from the continuous signal without affecting the signal itself using an ICA-based algorithm [7]. EEG fragments containing movement artifacts as well as any epileptic activity were removed based on visual inspection of the data. This resulted in an EEG signal clean from (eye) movement artifacts and epileptic activity, which was then used for further analysis. Afterwards, the continuous EEG signal was epoched according to the type of stimulus (Target and Non Target), with 200 ms pre-stimulus (delay period) and 400 ms poststimulus (presentation period of the second stimulus, where the motor responses had not yet taken place). Omitted Target trials (i.e. trials without correct motor response) and committed Non Target trials (i.e. trials with a wrong motor response) were excluded from the analysis. We then performed a down-sampling at 500 Hz and we applied a baseline correction by subtracting the mean value of the 200 ms of the pre-stimulus period. Overall, we ended up with 92 datasets (21 epileptic  $\times$  2 trial types + 25 control  $\times$  2 trial types) of 19 multi timeseries, which were divided into four group types (Epileptic- Target (ET), Epileptic-Non Target (ENT), Control-Target (CT), Control-Non Target (CNT)).

## 2.2 Numerical Solution of the Source localization Problem

Source localization aims at identifying the (unknown) sources of the brain from data taken usually from noninvasive electromagnetic recording (here: EEG recordings). Its solution involves a forward and an inverse problem. The forward problem refers to the calculation of the electric potentials of the electrodes starting from a given electrical source. The solution of the forward problem is related to the construction of a head model. The head model contains both anatomical information and the conductivities of three layers, namely the skull, the cortex and the scalp [46]. Anatomical images can be obtained experimentally with the aid of Magnetic Resonance Imaging (MRI) scans, while volume conduction models can be constructed using e.g. the Boundary Element Method (BEM) [47] or the Finite Elements Model method (FEM) [48]. The head model volume is tessellated into small-sized cubes, the voxels. Sources may be associated to single voxels or clusters of voxels. Here, each voxel is associated to a single source. The relation between the scalp recordings and the discretized head model volume is performed using the linear matrix equation:

$$\mathbf{V} = \mathbf{G}\mathbf{x} + \boldsymbol{\epsilon}, \quad (1)$$

where  $\mathbf{V}$  is a known  $N \times 1$  matrix which contains the time instances as recorded by each channel ( $N$  is the number of channels),  $\mathbf{x}$  is the unknown  $M \times 1$  matrix of the intensities of the  $M$  sources ( $M$  is the number of voxels).

The matrix  $\mathbf{G}$ , with dimensions  $N \times M$  is the so-called lead field matrix that contains the information of the head geometry and conductivities.  $\mathbf{G}$  is known (from the solution of the so called forward problem (see e.g. in [49])) and is related with the head model [50];  $\boldsymbol{\epsilon}$  reflects the noise in the measurements.

The inverse problem is ill-defined, as there is an infinite number of combinations of positions and intensities that could effectively produce the electric potentials and magnetic fields measured. The general idea behind its solution is to express it as a linear optimization problem with regularization:

$$\hat{\mathbf{x}} = \min_{\mathbf{x}} (||\mathbf{V} - \mathbf{G}\mathbf{x}||_2^2 + \sum_{i=1}^k \alpha_i ||W_i \mathbf{x}||_p). \quad (2)$$

In the above,  $k$  is the number of regularization constraints (reflecting the a-priori physiological information); the matrix  $W$ ,  $M \times M$ , is a weighted matrix related to the imposed constraints;  $\alpha_i$  is the regularization parameter and denote the importance of every constraint.

For different choices of  $W$ ,  $k$  and  $p$  (reflecting the type of the norm), we get different methods.

Here, for our analysis, we used and compared three different [51] methods, namely the weighted Minimum Norm Estimation (wMNE), the standardized Low Resolution Electromagnetic Tomography (sLORETA) and the dynamic Statistical Parametric Mapping (dSPM) that are described below.

### 2.2.1 Weighted Minimum Norm Estimation

For  $W = I$  (the identity matrix) and  $p = 2$  (the  $L - 2$  norm) in 2 we get the Minimum Norm Estimation (MNE) [52]. MNE uses the mathematical assumption that the best solution, through the infinite set of solutions, is the one with the minimum norm. Despite the fact that MNE was the first method used to extract a 3D distributed solution, the simplicity of its assumption often leads to inadequate solutions. In particular, it has been shown, that this method fails in identifying deep sources [53]. Because of the minimum norm constraint, sources that are located in deep regions are moved closer to the cortex.

The wMNE method is a variation of the MNE that improves the problem of the mislocation of the deep sources. wMNE uses instead of the identity matrix, a diagonal matrix  $W_c$  that contains the weighting factors. From the multiple choices that can be chosen as weighted factors, usually  $W_c = \text{diag}(\|G_i\|_2)$  (for  $i=1,\dots,M$ ) is chosen [54]. Then, the unique solution is given by:

$$x_{wMNE} = LV, \quad (3)$$

where  $L = G^T(G^T G + \alpha W_c)^{-1}$  is called the inverse operator with dimensions  $(M \times N)$ .

### 2.2.2 The Dynamic Statistical Parametric Mapping

The Dynamic Statistical Parametric Mapping (dSPM) [39] is similar to the wMNE but uses a different regularization. dSPM computes the source estimates of the noise based on the noise covariance matrix  $C_\epsilon = \alpha H$  and normalizes the rows of the inverse operator.

$H = I - \frac{1}{\mathbf{1}^T \mathbf{1}}$  is the centering matrix and plays the role of the identity matrix in the measurement space. Then, from equation 3, the source estimates of the noise form a diagonal matrix:

$$C_{\hat{x}} = W_{dSPM} = LC_\epsilon L^T. \quad (4)$$

Thus, the dSPM solution is given by:

$$x_{dSPM} = L_{dSPM} V, \quad (5)$$

where  $L_{dSPM} = W_{dSPM} L$ .

### 2.2.3 Standardized Low Resolution Electromagnetic Tomography

sLORETA considers another source of variance, except from the covariance of the measurement noise  $C_\epsilon$ : the covariance of the actual sources  $C_x = I$ . Assuming that the activity of the actual sources and the noise of the measurements are uncorrelated and based on the linear relation of equation 1, we have:

$$C_V = GC_x G^T + C_\epsilon = GG^T + \alpha H. \quad (6)$$

Substituting equation 6 to 3, and taking into account the linear relation of equation 3, we can estimate the variation of the estimated sources as:

$$C_{\hat{x}} = LC_V L^T = L(GG^T + \alpha H)L^T = G^T(GG^T + \alpha H)^{-1}G. \quad (7)$$

The covariance of the estimated sources is equivalent to the Backus and Gilbert resolution matrix [55], which is given by plugging equation 1 into 3 and substituting the inverse operator to get:

$$\hat{x} = LGx = G^T(GG^T + \alpha H)Gx = Ax = C_{\hat{x}}x, \quad (8)$$

where  $A = LG$  is the resolution matrix.

In this case, the solution is given by:

$$x_{sLORETA} = L_{sLORETA} V, \quad (9)$$

where  $L_{sLORETA} = AL$ .

### 2.2.4 Head models for children

In our study, we did not have individual MRI scans for each child that participated to the experiment. Thus, in the absence of such specific information, we used age-specific MRI templates for children acquired from the “Neurodevelopmental MRI database” [56–59]. The goal of this database is to provide for research purposes, exactly in the absence of specific MRI scans, a series of age-appropriate average MRI reference templates and related information. Each template was constructed using identical procedures to facilitate comparisons across lifespan. The database consists of average templates (T1W and T2W), segmenting priors, and stereotaxic atlases [56]. The “Neurodevelopmental MRI Database” is available online (<http://jerlab.psych.sc.edu/NeurodevelopmentalMRIDatabase/>). The database is publicly available to researchers upon request for clinical and experimental studies of normal and pathological brain development. The data is shared under a Creative Commons Attribution-NonCommercial-NoDerivs 3.0 Unported License (CC BY-NC-ND 3.0; [http://creativecommons.org/licenses/by-nc-nd/3.0/deed.en\\_US](http://creativecommons.org/licenses/by-nc-nd/3.0/deed.en_US)). Using this database, we were able to construct an “average” age-specific head model for each child taking into account its age. For our study, we constructed 11 averaged head models (taking into account the database with head models of children between 6 and 16 years old, i.e. one “average” head model per year). In table 1, we provide information about the total number of MRI scans per age.

Age	6	7	8	9	10	11	12	13	14	15	16
<b>1.5T</b>	27	27	46	46	62	31	37	34	32	32	34
<b>3.0T</b>	10		19		16		15	11	30		13
<b>Combined</b>	37	27	56	46	72	31	47	34	42	32	44

Table 1: Total number of scans per age for 1.5T, 3.0T and combined average MRI templates. All 1.5T MRIs and part of 3.0T MRIs are included in the "Combined" column as in the original publications [56, 58]

Here, for the construction of the head models, as skull conductivities are age-dependent [60], we used different conductivity ratios (CR, cortex/skull) for every age-dependent model. The conductivity value for scalp and cortex was set to the standard value of 0.33 S/m [61]. Table 2 presents analytically the different conductivity ratios for every age [61].

Age	6	7-8	9-10	11-12	13-14	15-16
<b>CR</b>	15	20	30	40	50	60

Table 2: Conductivity ratios (cortex/skull) for every age-dependent head model. The standard conductivity value for scalp and cortex was set to 0.33 S/m [61].

## 3 Results

For our analysis, we used the BrainStorm toolbox for matlab [62]. The source-reconstructed time series were obtained by combining the EEG recordings with the appropriate (respect to the age of the subject) constructed MRI templates. From each template, we extracted three layers (scalp, inner skull, outer skull) and the source space (cortical surface). The number of vertices for each layer were set to 2562 vertices for each surface. Then, the volume conduction models were constructed in openMEEG software [63] which uses the BEM. The space resolution for the source model was set to 5124 voxels with fixed orientation perpendicular to the cortex surface.

Thus, the time series at the source level were reconstructed using wMNE, dSPM and sLORETA. The noise was computed from the raw EEG data using the pre-stimulus period for baseline correction and then the noise covariance matrix was calculated. A parameter that has to be determined is the “signal to noise ratio” (SNR). In Brainstorm, the computation of SNR is performed as in the original MNE software of Hamalainen [64]. The signal covariance matrix is “whitened” by the noise covariance matrix and the square root of the mean of its spectrum yields the average amplitude of SNR. The default value in Brainstorm is set to 3.

The main results of source localization procedure are presented analytically at table 3. For our illustrations, we have split the time period to three main intervals: the pre-stimulus period [-200ms 0ms), the period exactly after the stimulus [0ms - 199ms] and the post-stimulus period [200ms - 400ms). Our analysis reveals similar results when applying the different methods.

In Table 4 we also provide the numerical residuals for each method (the L2-norm ( $res = \|V - G\hat{x}\|_2$ , where  $G$  is the forward operator and  $\hat{x}$  the estimated amplitudes), as well as the corresponding values of the regularization terms.

Time period	Method	CT	CNT	ET	ENT
<b>pro-stimulus</b> (-200ms - -1ms)	wMNE	-Right occipital lobe (~140 voxels)	-Occipital lobe (~100 voxels)	-Right occipital lobe (~90 voxels)	-Occipital lobe (~80 voxels)
	dSPM	-Right occipital lobe (~220 voxels)	-Right occipital lobe (~150 voxels)	-Right occipital lobe (~160 voxels)	-Occipital lobe (~190 voxels)
	sLORETA	-Right occipital lobe (~530 voxels)	-Occipital lobe (~230 voxels) -Left parietal lobe (~150 voxels)	-Right occipital lobe (~290 voxels)	-Right occipital lobe (~270 voxels)
<b>exactly after stimulus</b> 0ms - 199ms	wMNE	-Occipital lobe (~120 voxels)	-Right occipital lobe (~100 voxels)	-Occipital lobe (~90 voxels)	-Superior parietal lobe (~50 voxels) -Occipital lobe (~110 voxels)
	dSPM	-Right occipital lobe (~330 voxels)	-Right occipital lobe (~310 voxels)	-Occipital lobe (~240 voxels)	-Superior parietal lobe (~100 voxels) -Right occipital lobe (~330 voxels)
	sLORETA	-Right occipital lobe (~590 voxels)	-Occipital lobe (~510 voxels)	-Occipital lobe (~450 voxels)	-Superior parietal lobe (~240 voxels) -Occipital lobe (~500 voxels)
<b>post-stimulus</b> 200ms - 399ms	wMNE	-Parietal lobe (~70 voxels)	-Right parietal lobe (~60 voxels)	-Right parietal lobe (~60 voxels)	-Right parietal lobe (~80 voxels)
	dSPM	-Parietal lobe (~180 voxels)	-Parietal lobe (~110 voxels)	-Right parietal lobe (~200 voxels)	-Parietal lobe (~190 voxels)
	sLORETA	-Parietal lobe (~390 voxels)	-Parietal lobe (~360 voxels)	-Right parietal lobe (~470 voxels)	-Parietal lobe (~500 voxels)

Table 3: Group averaged sources as obtained by the three methods: wMNE, dSPM and sLORETA. CT: Control Target, CNT: Control non-Target, ET: Epileptic Target, ENT: Epileptic non-Target.

Method	Group	Residuals ( $\mu\text{V}$ )	Regularization term (nA-m)
<b>wMNE</b>	CT	4.53±0.94	13.2±2.14
	ET	5.34±1.02	15.41±3.23
	CNT	3.63±1.25	13.13±3.42
	ENT	6.42±1.76	16.31±3.67
<b>dSPM</b>	CT	3.92±0.71	12.78±3.12
	ET	5.21±1.18	15.91±3.54
	CNT	4.11±1.37	14.34±4.15
	ENT	7.08±1.58	17.37±4.52
<b>sLORETA</b>	CT	3.12±0.59	10.91±3.19
	ET	4.04±0.86	11.46±2.84
	CNT	2.98±0.43	11.51±2.9
	ENT	3.45±0.73	12.43±3.57

Table 4: Mean and standard deviation values for the L2-norm residuals and the regularization term for each method and each group.

### 3.1 Hypothesis Testing Using T-test

After the data pre-processing and the implementation of the source-localization algorithms, as described in the previous section, we got 92 time-series at the source space. Our data have a spatio-temporal structure: number of voxels (spatial dimension) and time points (time dimension). In order to perform two-sample T-tests for the identification of statistically significant differences in the activity of the sources among groups, we checked three basic assumptions. In particular, we checked if (1) the amplitude of the source signal at each voxel and at each time instant follows a normal distribution among subjects in a group, (2) the variances of the amplitude of the source signal at each voxel and at each time instant of CT, ET and CNT, ENT are equal, and (3) the amplitudes of the source signal at each voxel and at each time instant are independent for CT, ET and CNT, ENT.

For the test of normality, we used the Shapiro-Wilk test [65]. The null hypothesis of the test is that a sample comes from a normal distribution. The test statistic reads:

$$W = \frac{(\sum_{i=1}^n \alpha_i x_{(i)})^2}{\sum_{i=1}^n (x_i - \bar{x})^2}, \quad (10)$$

where  $x_{(i)}$  is the  $i$ -th order statistic,  $\bar{x}$  is the sample mean and coefficients  $\alpha_i$  are given by  $(\alpha_1, \alpha_2, \dots, \alpha_n) = \frac{m^T V^{-1}}{C}$ .  $C$  is a vector norm  $C = \|V^{-1}m\| = (m^T V^{-1} V^{-1} m)^{\frac{1}{2}}$ ,  $m = (m_1, m_2, \dots, m_n)^T$  are the expected values of the order statistics of independent and identically distributed random variables sampled from the standard normal distribution and  $V$  is the covariance matrix of those normal order statistics. F-tests were performed to validate the second assumption (i.e. the equality of the variances of the amplitude values of each voxel between ET and CT and between ENT and CNT).

Thus, we tested for normality and equality of variances for each voxel and each time sample (i.e. we have performed a total of  $5.148 \times 600 = 3.088.800$  t-tests). The level of significance was set to  $p < 0.05$ , meaning that the risk of taking a false positive is 5% of the cases. Here, in order to deal with the multicomparison problem, we used the false discovery rate (FDR) correction [66]. Following this procedure, the null hypothesis could not be rejected. Similarly, the F tests validated also the second assumption. The independence is reasonably assumed to hold true.

Having guaranteed that the T-test can be applied, we proceeded with the comparisons ET vs CT and ENT vs CNT. The null hypothesis  $H_0$  for both comparisons was that the two groups have equal means regarding the emerged spatio-temporal activation at the source level. Again, we performed  $3.E^6$  simultaneous two-sample T-tests with  $p < 0.05$  level of significance. FDR was used to deal with the multicomparison problem. Another constraint that we added to avoid spurious and random effects was the one of the minimum duration of the activations. Thus, we excluded all the signals that were statistically significant for time intervals less than 50 ms. This statistical analysis revealed that all methods gave relatively similar results. The pair T-test between ENT and CNT revealed a statistically significant difference in the time-range of 170ms-230ms. In this time-range, the Superior Parietal Lobe (SPL) was activated more in the ENT group; the activation of the SPL was mostly at the right hemisphere (figure 1). The pair T-test between ET and CT revealed a statistically significant difference in the time-range of 160ms-360ms. In this time-range the Inferior Parietal Lobule (IPL) was activated more in the ET group (only at the right hemisphere) (figure 2).

The above findings are summarized in Table 5.

Comparison	Time period	Group activated more	Brain region	Brodman area	Number of voxels	Comments
ENT vs CNT	170-230	ENT	SPL	7	~80	Only at the right hemisphere
ET vs CT	160-360	ET	IPL	22, 39-40	~170	Only at the right hemisphere

Table 5: Analytical presentation of the differences between the comparisons ET vs CT and ENT vs CNT.



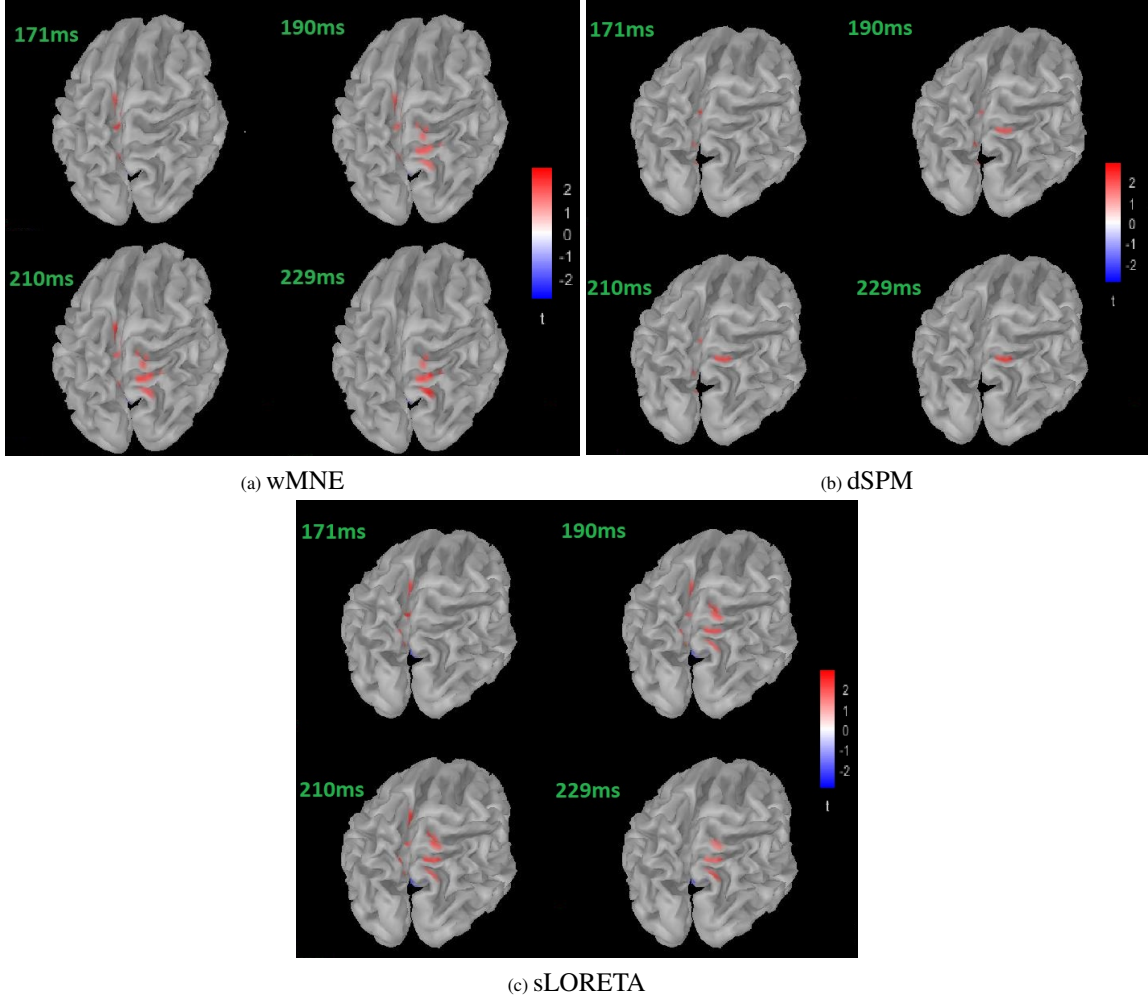


Figure 1: ENT vs CNT: SPL mainly of the right hemisphere activate more for the ENT group at the time interval from 170 to 230 ms.

## 4 Conclusions

Sensor-level analysis does not provide information about the actual sources that are involved in brain activity. From a mathematical point of view, the problem of source localization from scalp recordings is an inverse ill-defined problem and as such, different types of regularization approaches may in principle result to different solutions. Thus, especially for clinical assessment of brain neurological disorders such as epilepsy, there is a need for comparing and assessing the robustness of such methods.

This is the first study to perform a comparative analysis of three numerical methods, namely the sLORETA, wMNE and dSPM to identify differences at the source level between healthy children and children with well-controlled epilepsy (i.e. in the absence of seizures) during a working memory task. In the absence of anatomical MRI scans, we used the publicly “Neurodevelopmental MRI database” that provides age-specific average MRI templates. Our analysis shows that all three methods yield essentially the same results, thus providing adequate confidence for our findings. More specifically, our analysis revealed consistent differences between the two groups in the parietal lobes. Importantly, our findings are in line with other studies investigating abnormalities of the brain function due to epilepsy with the use of anatomical MRI, fMRI and EEG recordings [67–76]. More specifically, regarding children with epilepsy, Besenyi et al. [76] used anatomical MRI and resting state EEG recordings to identify the abnormal brain activity in children with benign rolandic epilepsy. Using LORETA, they found an increase activity, compared to controls, in the temporal and inferior parietal lobule. Other studies that have investigated the abnormal activity in children with epilepsy in the presence of seizures have also pinpointed the importance of these areas. Clemens et al. ([77] find increased activity in

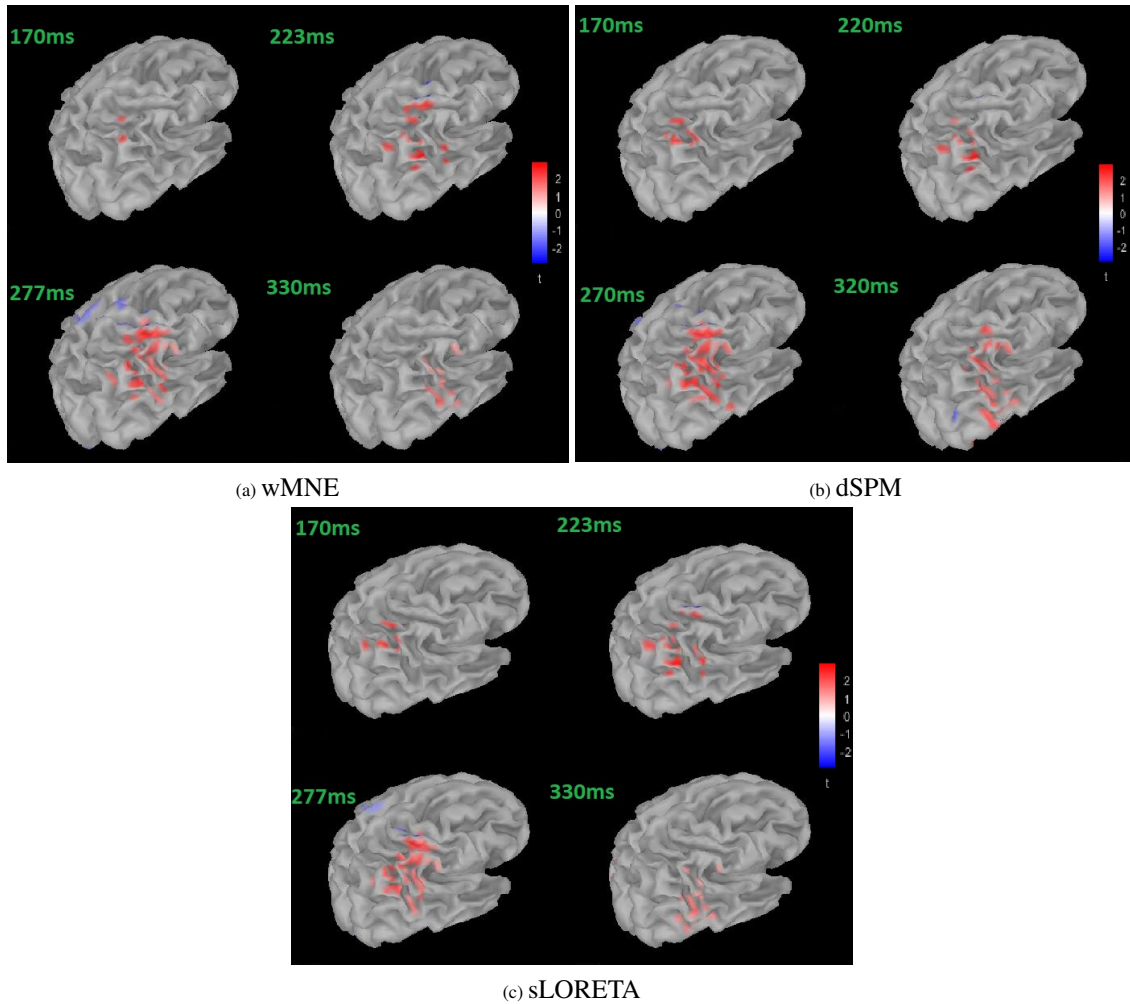


Figure 2: ET vs CT: IPL of the right hemisphere activates more for the ET group at the time interval from 160 to 360 ms.

the superior parietal lobe children with benign childhood epilepsy with rolandic spikes, using MRI scans and resting state EEG recordings. For the source localization analysis they used LORETA.

Importantly, our study and findings reveal also the importance and potential that originates from the use of publicly available scientific resources such as the “Neurodevelopmental MRI” database, which allow to the researchers to re-analyse available neuroimaging data and investigate questions beyond the scope of the original studies. This carries, in principle, the potential to gain new insights without the need to perform new from scratch, time-consuming and expensive experiments.

## Acknowledgments

E.G. was supported by a Ph.D. fellowship by the Department of Mathematics and Applications, University of Naples Federico II and I.G. was supported by a Ph.D. fellowship by the National Technical University of Athens.

## Conflict of interest

All authors declare no conflicts of interest in this paper

## References

- [1] Kari Modalsli Aaberg, Nina Gunnes, Inger Johanne Bakken, Camilla Lund Søråas, Aleksander Berntsen, Per Magnus, Morten I. Lossius, Camilla Stoltenberg, Richard Chin, and Pål Surén. Incidence and prevalence of childhood epilepsy: A nationwide cohort study. *Pediatrics*, 139(5):e20163908, April 2017.
- [2] Sharon Davies, Isobel Heyman, and Robert Goodman. A population survey of mental health problems in children with epilepsy. *Developmental Medicine & Child Neurology*, 45(05), April 2003.
- [3] Douglas S. Goodin, Michael J. Aminoff, and Kenneth Laxer. Detection of epileptiform activity by different noninvasive eeg methods in complex partial epilepsy. *Annals of neurology*, 27:330–4, 03 1990.
- [4] S J M Smith. Eeg in the diagnosis, classification, and management of patients with epilepsy. *Journal of Neurology, Neurosurgery and Psychiatry*, 76(suppl 2):ii2–ii7, 2005.
- [5] Mohammed M. S. Jan, Mark Sadler, and Susan R. Rahey. Lateralized postictal eeg delta predicts the side of seizure surgery in temporal lobe epilepsy. *Epilepsia*, 42(3):402–405, 2001.
- [6] Christina M. Krause, Petra-Ann Boman, Lauri Sillanmäki, Tarja Varho, and Irma E. Holopainen. Brain oscillatory eeg event-related desynchronization (erd) and -synchronization (ers) responses during an auditory memory task are altered in children with epilepsy. *Seizure*, 17(1):1 – 10, 2008.
- [7] Ivan Myatchin, Maarten Mennes, Heidi Wouters, Peter Stiers, and Lieven Lagae. Working memory in children with epilepsy: An event-related potentials study. *Epilepsy Research*, 86:183–190, 2009.
- [8] Foteini Protopapa, Constantinos I. Siettos, Ioannis Evdokimidis, and Nikolaos Smyrnis. Granger causality analysis reveals distinct spatio-temporal connectivity patterns in motor and perceptual visuo-spatial working memory. *Frontiers in Computational Neuroscience*, 8:146, 2014.
- [9] Li Yang, Irina Shklyar, Hyang Woon Lee, Celestine C. Ezeani, Joseph Anaya, Samantha Balakirsky, Xiao Han, Sheila Enamandram, Clara Men, Joyce Y. Cheng, Abigail Nunn, Tanya Mayer, Czestochowa Francois, Molly Albrecht, Alan L. Hutchison, Ee-Lynn Yap, Kevin Ing, Gvantsa Didebulidze, Bo Xiao, Hamada Hamid, Pue Farooque, Kamil Detyniecki, Joseph T. Giacino, and Hal Blumenfeld. Impaired consciousness in epilepsy investigated by a prospective responsiveness in epilepsy scale (res). *Epilepsia*, 53(3):437–447, 2012.
- [10] Eric van Diessen, Willem M. Otte, Kees P. J. Braun, Cornelis J. Stam, and Floor E. Jansen. Improved diagnosis in children with partial epilepsy using a multivariable prediction model based on eeg network characteristics. *PLOS ONE*, 8(4):1–8, 04 2013.
- [11] Chris Plummer, A. Simon Harvey, and Mark Cook. EEG source localization in focal epilepsy: Where are we now? *Epilepsia*, 49(2):201–218, February 2008.
- [12] Pierre Mégevand and Margitta Seeck. Electroencephalography, magnetoencephalography and source localization. *Current Opinion in Neurology*, 31(2):176–183, April 2018.
- [13] Kitti Kaiboriboon, Hans O. Lüders, Mehdi Hamaneh, John Turnbull, and Samden D. Lhatoo. EEG source imaging in epilepsy—practicalities and pitfalls. *Nature Reviews Neurology*, 8(9):498–507, August 2012.
- [14] John S. Ebersole and Susan M. Ebersole. Combining MEG and EEG source modeling in epilepsy evaluations. *Journal of Clinical Neurophysiology*, 27(6):360–371, December 2010.
- [15] Friederike Moeller, Ulrich Stephani, and Michael Siniatchkin. Simultaneous EEG and fMRI recordings (EEG-fMRI) in children with epilepsy. *Epilepsia*, 54(6):971–982, May 2013.
- [16] Munsif Ali Jatoi, Nidal Kamel, Aamir Saeed Malik, and Ibrahima Faye. Eeg based brain source localization comparison of sloreta and eloreta. *Australasian Physical & Engineering Sciences in Medicine*, 37(4):713–721, Dec 2014.
- [17] F. Cincotti, C. Babiloni, C. Miniussi, F. Carducci, D. Moretti, S. Salinari, R. Pascual-Marqui, P. M. Rossini, and F. Babiloni. EEG deblurring techniques in a clinical context. *Methods of Information in Medicine*, 43(01):114–117, 2004.
- [18] Jun Yao and Julius P.A. Dewald. Evaluation of different cortical source localization methods using simulated and experimental EEG data. *NeuroImage*, 25(2):369–382, apr 2005.
- [19] Yohan Attal and Denis Schwartz. Assessment of subcortical source localization using deep brain activity imaging model with minimum norm operators: A MEG study. *PLoS ONE*, 8(3):e59856, mar 2013.
- [20] Anett Seeland, Mario M. Krell, Sirko Straube, and Elsa A. Kirchner. Empirical comparison of distributed source localization methods for single-trial detection of movement preparation. *Frontiers in Human Neuroscience*, 12, sep 2018.

- [21] Andreas A. Ioannides, Lichan Liu, Vahe Poghosyan, Khalid Hamandi, and George K. Kostopoulos. Source-estimation from non-invasive recordings of brain electrical activity in sleep and epilepsy. In *Cyberphysical Systems for Epilepsy and Related Brain Disorders*, pages 61–86. Springer International Publishing, 2015.
- [22] R.A. Chowdhury, I. Merlet, G. Birot, E. Kobayashi, A. Nica, A. Biraben, F. Wendling, J.M. Lina, L. Albera, and C. Grova. Complex patterns of spatially extended generators of epileptic activity: Comparison of source localization methods cMEM and 4-ExSo-MUSIC on high resolution EEG and MEG data. *NeuroImage*, 143:175–195, dec 2016.
- [23] Mahmoud Hassan, Isabelle Merlet, Ahmad Mheich, Aya Kabbara, Arnaud Biraben, Anca Nica, and Fabrice Wendling. Identification of interictal epileptic networks from dense-EEG. *Brain Topography*, 30(1):60–76, aug 2016.
- [24] Azeez Adebimpe, Ardalan Aarabi, Emilie Bourel-Ponchel, Mahdi Mahmoudzadeh, and Fabrice Wallois. EEG resting state functional connectivity analysis in children with benign epilepsy with centrotemporal spikes. *Frontiers in Neuroscience*, 10, March 2016.
- [25] Kristina Groening, Verena Brodbeck, Friederike Moeller, Stephan Wolff, Andreas van Baalen, Christoph M. Michel, Olav Jansen, Rainer Boor, Gert Wiegand, Ulrich Stephani, and Michael Siniatchkin. Combination of EEG–fMRI and EEG source analysis improves interpretation of spike-associated activation networks in paediatric pharmacoresistant focal epilepsies. *NeuroImage*, 46(3):827–833, July 2009.
- [26] Lydia Elshoff, Kristina Groening, Frédéric Grouiller, Gert Wiegand, Stephan Wolff, Christoph Michel, Ulrich Stephani, and Michael Siniatchkin. The value of EEG–fMRI and EEG source analysis in the presurgical setup of children with refractory focal epilepsy. *Epilepsia*, 53(9):1597–1606, July 2012.
- [27] P Fergus, David Hignett, Abir Hussain, Dhiya Al-Jumeily, and Khaled Abdel-Aziz. Automatic epileptic seizure detection using scalp eeg and advanced artificial intelligence techniques. *BioMed Research International*, 2015:17, 01 2015.
- [28] H. L. Swanson. Cross-sectional and incremental changes in working memory and mathematical problem solving. *Journal of Educational Psychology*, 98(2):265 – 281, 2006.
- [29] Susan E. Gathercole, Susan J. Pickering, Camilla Knight, and Zoe Stegmann. Working memory skills and educational attainment: evidence from national curriculum assessments at 7 and 14 years of age. *Applied Cognitive Psychology*, 18(1):1–16, 2004.
- [30] Susan E. Gathercole, Tracy P. Alloway, Hannah J. Kirkwood, Julian G. Elliott, Joni Holmes, and Kerry A. Hilton. Attentional and executive function behaviours in children with poor working memory. *Learning and Individual Differences*, 18(2):214 – 223, 2008.
- [31] Jozsef A. Toth and Michael Lewis. The role of working memory and external representation in individual decision making. *AAAI Technical Report*, 11, 05 2003.
- [32] Christian C. Ruff, Markus Knauff, Thomas Fangmeier, and Joachim Spreer. Reasoning and working memory: common and distinct neuronal processes. *Neuropsychologia*, 41(9):1241 – 1253, 2003.
- [33] Sibel G?lg?nen, Veysi Demirbilek, Bari? Korkmaz, Ay?m Dervent, and Brenda D. Townes. Neuropsychological functions in idiopathic occipital lobe epilepsy. *Epilepsia*, 41(4):405–411, 2000.
- [34] Yves Chaix, Virginie Laguitton, Val?rie Lauwers-Canc?s, G?raldine Daquin, Claude Canc?s, Jean-Fran?ois D?monet, and Nathalie Villeneuve. Reading abilities and cognitive functions of children with epilepsy: Influence of epileptic syndrome. *Brain and Development*, 28(2):122 – 130, 2006.
- [35] Pablo Campo, Fernando Maest?, Irene Garc?a-Morales, Antonio Gil-Nagel, Bryan Strange, Manuel Morales, and Tom?s Ortiz. Modulation of medial temporal lobe activity in epilepsy patients with hippocampal sclerosis during verbal working memory. *Journal of the International Neuropsychological Society : JINS*, 15:536–46, 08 2009.
- [36] Dylan D. Wagner, Viviane Sziklas, Krista E. Garver, and Marilyn Jones-Gotman. Material-specific lateralization of working memory in the medial temporal lobe. *Neuropsychologia*, 47(1):112 – 122, 2009.
- [37] Lindsay M. Luton, Thomas G. Burns, and Nick DeFilippis. Frontal Lobe Epilepsy in Children and Adolescents: A Preliminary Neuropsychological Assessment of Executive Function. *Archives of Clinical Neuropsychology*, 25(8):762–770, 09 2010.
- [38] Roberto D. Pascual-Marqui. Standardized low-resolution brain electromagnetic tomography (sloreta): technical details. *Methods and findings in experimental and clinical pharmacology*, 24D:5–12, 2002.
- [39] Anders M. Dale, Arthur K. Liu, Bruce R. Fischl, Randy L. Buckner, John W. Belliveau, Jeffrey D. Lewine, and Eric Halgren. Dynamic statistical parametric mapping: Combining fmri and meg for high-resolution imaging of cortical activity. *Neuron*, 26(1):55 – 67, 2000.

- [40] Sunao Iwaki and Shoogo Ueno. Weighted minimum-norm source estimation of magnetoencephalography utilizing the temporal information of the measured data. *Journal of Applied Physics*, 83:6441–6443, 06 1998.
- [41] Yuki Otsuka, Naoyuki Osaka, and Mariko Osaka. Functional asymmetry of superior parietal lobule for working memory in the elderly. *Neuroreport*, 19:1355–9, 10 2008.
- [42] Michael Koenigs, Aron K. Barbey, Bradley R. Postle, and Jordan Grafman. Superior parietal cortex is critical for the manipulation of information in working memory. *Journal of Neuroscience*, 29(47):14980–14986, 2009.
- [43] Ingrid R. Olson and Marian Berryhill. Some surprising findings on the involvement of the parietal lobe in human memory. *Neurobiology of Learning and Memory*, 91(2):155 – 165, 2009. Special Issue: Parietal Cortex.
- [44] Susan Ravizza, Marlene Behrmann, and Julie Fiez. Right parietal contributions to verbal working memory: Spatial or executive? *Neuropsychologia*, 43:2057–67, 02 2005.
- [45] Arnaud Delorme and Scott Makeig. Eeglab: an open source toolbox for analysis of single-trial eeg dynamics including independent component analysis. *Journal of Neuroscience Methods*, 134(1):9 – 21, 2004.
- [46] Asta Kybartaite. Computational representation of a realistic head and brain volume conductor model: electroencephalography simulation and visualization study. *International Journal for Numerical Methods in Biomedical Engineering*, 28(11):1144–1155, 2012.
- [47] Manfred Fuchs, Michael Wagner, and Jörn Kastner. Boundary element method volume conductor models for eeg source reconstruction. *Clinical Neurophysiology*, 112(8):1400 – 1407, 2001.
- [48] Carsten H. Wolters. The finite element method in eeg/meg source analysis. 2007.
- [49] Hans Hallez, Bart Vanrumste, Roberta Grech, Joseph Muscat, Wim De Clercq, Anneleen Vergult, Yves D’Asseler, Kenneth P. Camilleri, Simon G. Fabri, Sabine Van Huffel, and Ignace Lemahieu. Review on solving the forward problem in eeg source analysis. *Journal of NeuroEngineering and Rehabilitation*, 4(1):46, Nov 2007.
- [50] Roberto D Pascual-Marqui and Rolando Jose Lirio. Spatial resolution of neuronal generators based on eeg and meg measurements. *The International journal of neuroscience*, 68:93–105, 02 1993.
- [51] Anett Seeland, Mario M. Krell, Sirko Straube, and Elsa A. Kirchner. Empirical comparison of distributed source localization methods for single-trial detection of movement preparation. *Frontiers in Human Neuroscience*, 12:340, 2018.
- [52] M. S. Hämmäläinen and R. J. Ilmoniemi. Interpreting magnetic fields of the brain: minimum norm estimates. *Medical & Biological Engineering & Computing*, 32(1):35–42, Jan 1994.
- [53] Matti Stenroos and Olaf Hauk. Minimum-norm cortical source estimation in layered head models is robust against skull conductivity error. *NeuroImage*, 81:265 – 272, 2013.
- [54] Roberta Grech, Tracey Cassar, Joseph Muscat, Kenneth P. Camilleri, Simon G. Fabri, Michalis Zervakis, Petros Xanthopoulos, Vangelis Sakkalis, and Bart Vanrumste. Review on solving the inverse problem in eeg source analysis. *Journal of NeuroEngineering and Rehabilitation*, 5(1):25, Nov 2008.
- [55] George Backus and Freeman Gilbert. The Resolving Power of Gross Earth Data. *Geophysical Journal International*, 16(2):169–205, 10 1968.
- [56] John E. Richards, Carmen Sanchez, Michelle Phillips-Meek, and Wanze Xie. A database of age-appropriate average mri templates. *NeuroImage*, 124:1254–1259, 2016.
- [57] Alan C. Evans. The nih mri study of normal brain development. *NeuroImage*, 30(1):184 – 202, 2006.
- [58] Carmen E. Sanchez, John E. Richards, and C. Robert Almlı. Age-specific mri templates for pediatric neuroimaging. *Developmental Neuropsychology*, 37(5):379–399, 2012. PMID: 22799759.
- [59] John E. Richards and Wanze Xie. Chapter one - brains for all the ages: Structural neurodevelopment in infants and children from a life-span perspective. volume 48 of *Advances in Child Development and Behavior*, pages 1 – 52. JAI, 2015.
- [60] Katrina Wendel-Mitoraj, Juho V?is?nen, Gunnar Seemann, Jari Hyttinen, and Jaakko Malmivuo. The influence of age and skull conductivity on surface and subdermal bipolar eeg leads. *Computational Intelligence and Neuroscience*, 2010:397272, 01 2010.
- [61] Hannah McCann, Giampaolo Pisano, and Leandro Beltrachini. Variation in reported human head tissue electrical conductivity values. *Brain Topography*, 32(5):825–858, Sep 2019.
- [62] Sylvain Baillet, John Mosher, R.M. Leahy, and D.W. Shattuck. Brainstorm: A matlab toolbox for the processing of meg and eeg signals. *NeuroImage*, 9:S246, 01 1999.

- [63] Alexandre Gramfort, Th?odore Papadopoulos, Emmanuel Olivi, and Maureen Clerc. Openmeeg: Opensource software for quasistatic bioelectromagnetics. *Biomedical engineering online*, 9:45, 09 2010.
- [64] Alexandre Gramfort, Martin Luessi, Eric Larson, Denis Engemann, Daniel Strohmeier, Christian Brodbeck, Lauri Parkkonen, and Matti H?m?inen. Mne software for processing meg and eeg data. *NeuroImage*, 86, 10 2013.
- [65] Ahmed BenSaida. Shapiro-wilk and shapiro-francia normality tests. *MATLAB Central File Exchange*. <https://www.mathworks.com/matlabcentral/fileexchange/13964-shapiro-wilk-and-shapiro-francia-normality-tests>), December 2019.
- [66] Yoav Benjamini and Yosef Hochberg. Controlling the false discovery rate - a practical and powerful approach to multiple testing. *J. Royal Statist. Soc., Series B*, 57:289 – 300, 11 1995.
- [67] Marian E. Berryhill and Ingrid R. Olson. Is the posterior parietal lobe involved in working memory retrieval?: Evidence from patients with bilateral parietal lobe damage. *Neuropsychologia*, 46(7):1775 – 1786, 2008. Part Special Issue: What is the Parietal Lobe Contribution to Human Memory?
- [68] Kevin Jones and Marian Berryhill. Parietal contributions to visual working memory depend on task difficulty. *Frontiers in Psychiatry*, 3:81, 2012.
- [69] Mariko Osaka, Mie Komori, Masanao Morishita, and Naoyuki Osaka. Neural bases of focusing attention in working memory: An fmri study based on group differences. *Cognitive, affective and behavioral neuroscience*, 7:130–9, 07 2007.
- [70] Song Li, Jing-Na Jin, Xin Wang, Hong-Zhi Qi, Zhi-Peng Liu, and Tao Yin. Theta and alpha oscillations during the retention period of working memory by rtms stimulating the parietal lobe. *Frontiers in Behavioral Neuroscience*, 11:170, 2017.
- [71] Juan CH Tseng P, Iu KC. The critical role of phase difference in theta oscillation between bilateral parietal cortices for visuospatial working memory. *Scientific reports*, 8(1):349, 01 2018.
- [72] Bruce Hermann, Jana Jones, Raj Sheth, Christian Dow, Monica Koehn, and Michael Seidenberg. Children with new-onset epilepsy: neuropsychological status and brain structure. *Brain*, 129(10):2609–2619, 08 2006.
- [73] Chong-Yu Hu, Xiaoping Gao, Lili Long, Xiaoyan Long, Chaorong Liu, Yayu Chen, Yuanyuan Xie, Chujuan Liu, Bo Xiao, and Zhe-Yu Hu. Altered dmn functional connectivity and regional homogeneity in partial epilepsy patients: a seventy cases study. *Oncotarget*, 8(46):81475–81484, 2017.
- [74] Kerstin H. Kipp, Bertram Opitz, Martina Becker, Juliane Hofmann, Christoph Krick, Ludwig Gortner, and Alex Mecklinger. Neural correlates of recognition memory in children with febrile seizures: Evidence from functional magnetic resonance imaging. *Frontiers in human neuroscience*, 6:17, 02 2012.
- [75] Lars Michels, Kerstin Bucher, Rafael L?chinger, Peter Klaver, Ernst Martin, Daniel Jeanmonod, and Daniel Brandeis. Simultaneous eeg-fmri during a working memory task: Modulations in low and high frequency bands. *PLOS ONE*, 5(4):1–15, 04 2010.
- [76] M. Besenyei, E. Varga, I. Fekete, S. Puskás, K. Hollódy, A. Fogarasi, M. Emri, G. Opposits, S.A. Kis, and B. Clemens. EEG background activity is abnormal in the temporal and inferior parietal cortex in benign rolandic epilepsy of childhood: A LORETA study. *Epilepsy Research*, 98(1):44–49, jan 2012.
- [77] Béla Clemens, Szilvia Puskás, Tamás Spisák, Imre Lajtos, Gábor Opposits, Mónika Besenyei, Katalin Hollódy, András Fogarasi, Noémi Zsuzsanna Kovács, István Fekete, and Miklós Emri. Increased resting-state EEG functional connectivity in benign childhood epilepsy with centro-temporal spikes. *Seizure*, 35:50–55, feb 2016.